A Simple Statistical Mechanical Model of Water

Thomas M. Truskett[†,‡] and Ken A. Dill[†]

Department of Pharmaceutical Chemistry, University of California, San Francisco, San Francisco, California 94143-1204, Department of Chemical Engineering, The University of Texas at Austin, Austin, Texas 78712-1062, and Institute for Theoretical Chemistry, The University of Texas at Austin, Austin, Texas 78712

Received: June 13, 2002; In Final Form: September 10, 2002

We introduce a statistical mechanical model for the physical properties of water. Each water molecule is a two-dimensional disk with three radial hydrogen-bonding arms. Energetic interactions are based on water triplets, a central water molecule interacting with two neighbors via hydrogen bonds, van der Waals attractions, and steric repulsions. Interactions with more distant molecules are treated in a mean-field way. Each molecular triplet can be in one of three energy levels: cage-like hydrogen-bonded structures, denser nonbonded structures, and expanded structures with no near-neighbor interactions. The model predicts water's thermodynamic anomalies, including maxima in density, minima in isothermal compressibility and heat capacity, and expansion upon freezing at low pressure. It predicts the main features of water's phase diagram, including multiple crystalline phases and the proposed liquid−liquid transition in supercooled water. Also, it captures qualitatively the fragile-to-strong transition in the liquid's temperature-dependent relaxation processes. This model is intended to give simple insights into the microscopic origins of water's distinctive physical properties.

I. Introduction

Many important insights have come from atomically detailed computer simulations of liquids and solids. But complementary insights have come from simpler models that can be treated analytically. Physical chemistry textbooks often develop analytical models such as the ideal gas and the van der Waals fluid for several reasons: (1) physical properties can be calculated from analytical models without sophisticated computational methods, (2) some of these physical properties, in particular those involving entropies, heat capacities, or phase changes, are difficult to access by simulations of detailed models because of sampling limitations, and (3) analytical models can lead to functional forms for the dependencies of properties on molecular parameters and independent variables, tools that are useful for engineering applications. In that spirit we develop here an analytical treatment of a highly simplified model for the physical properties of water.

Water is considered to be anomalous among liquids. Compared to molecules of similar size,[1] water has higher freezing, boiling, and critical temperatures, surface tension, heat of vaporization, and isobaric heat capacity. Liquid water also has "density anomalies" at atmospheric pressure: it is denser than its solid phase (ice I_h), its density passes through a maximum at 4 °C, and it continues to expand when cooled to lower temperatures.

Moreover, temperature and pressure affect "hot" water (near its boiling point) differently than "cold" water (near its freezing point). Heating hot water increases its isothermal compressibility and isobaric heat capacity and reduces its density and refractive index. Heating cold water has the opposite effect.[2] Applied pressure reduces the mobility of the molecules in hot water, but it increases the mobility of cold water.[3] Pressure melts ice at low pressures and freezes the liquid at high pressures. Liquid water's anomalies become more pronounced when it is supercooled, i.e., cooled below its freezing temperature without crystallization. For example, supercooling leads to sharp increases in its isothermal compressibility, isobaric heat capacity, and the magnitude of its (negative) thermal expansion coefficient. Power-law extrapolations predict that these rapidly growing response functions would diverge just below the lowest temperature where liquid-state measurements are possible (ca. −38 °C at atmospheric pressure),[4−6] suggesting the possibility of a thermodynamic singularity in the deeply supercooled liquid.[6]

Also, liquid water participates in hydrophobic interactions with nonpolar molecules. These interactions are important for many self-organization and aggregation processes in aqueous solution, including protein folding, the formation of surfactant assemblies, lipid bilayers, and cell membranes, and the binding of drugs to proteins.[7−12] Some insightful theoretical treatments[10,13−16] suggest that key aspects of hydrophobic hydration are related to the distinctive thermodynamics of pure water. Hence, a good starting point for studying water's role in solvation−desolvation processes is to understand the properties of water itself.

We recently introduced a simple analytical theory for water[17] that is able to predict qualitatively pure water's distinctive behavior from a microscopic model of its hydrogen bonds, van der Waals attractions, and steric repulsions. Our aim here is to develop that model and to use it to explore the plausible microscopic origins of water's distinctive physical properties.

II. Theory

A. Two-Dimensional Radial Arm Models. Ours is a two-dimensional radial arm model (2DRAM) (see Figure 1).[18] In

[†] University of California.
[‡] The University of Texas at Austin (permanent address).

10.1021/jp021418h CCC: $22.00
Published on Web 10/22/2002

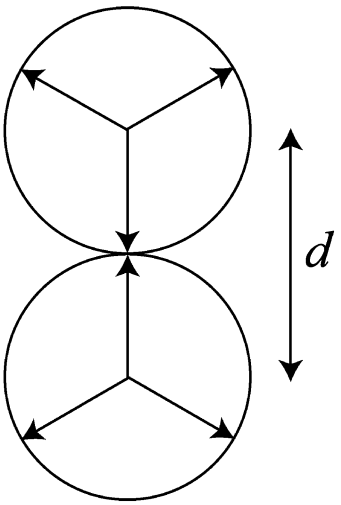

Figure 1. Geometry of a perfect hydrogen bond between two adjacent molecules in a 2DRAM.

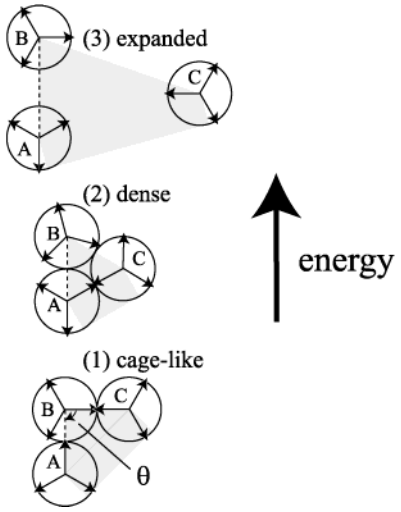

Figure 2. Cell types for the fluid states, shown from bottom to top in order of increasing energy. The cell volumes v_j ($j = 1-3$) are indicated by the gray shaded house-shaped regions. The triangle that forms the top of the house is defined by the lines that connect the three molecular centers of A, B, and C. The base of the house is the rectangle that lies between the line connecting molecular centers of A and C and the parallel line tangent to those molecules. The molecular sectors in one cell sum exactly to the volume of one molecule $\pi d^2/4$. θ is the local orientation of the "central" molecule B.

2DRAMs, each water molecule is a two-dimensional disk with three identical bonding arms, separated by 120°, as in the Mercedes Benz (MB) logo. Good hydrogen bonds are defined as shown in Figure 1: two arms of adjacent molecules are collinear and their molecular centers are separated by a distance *d*. This hydrogen-bond structure promotes orientationally constrained (low entropy) and open (low density) networks, which are regarded as key components of water's anomalous thermodynamic behavior.[19,20] One particular 2DRAM potential, the MB model, has been studied extensively by *NPT* Monte Carlo simulations.[21−27] Despite its simplicity, the MB model reproduces the general properties of liquid water, including negative thermal expansivity over a wide range of temperature and pressure, anomalously large isobaric heat capacity, minima in both heat capacity and isothermal compressibility upon isobaric cooling, and expansion upon freezing.[21,22] In addition, the MB model reproduces the experimental trends with temperature for the solvation of nonpolar solutes, including the free energy, entropy, enthalpy, molar volume, and heat capacity of transfer.[21] Because 2DRAMs can predict qualitatively the distinctive properties of water, and because they give insights into the underlying structural origins of those properties, we felt it would be valuable to develop an analytical version of this type of model. Hence, the molecules in our approach are two-dimensional disks of the type shown in Figure 1, although the details of the interactions are somewhat different from the MB model.

B. Variable-Cell Description of Water's Structure. Our model for water's liquid and vapor phases can be classified as a variable-structure cell theory. Cell theories have played a central role in the study of condensed-phase systems.[28−30] Their widespread use can be attributed to the fact that they have intuitive microscopic formulations and generate qualitatively correct thermodynamic predictions. A key assumption in these approaches is that each molecule in the system is confined by its neighbors to a localized region of space called a *cell*. In such theories, the cells are independent and geometrically identical, an approximation that is based on the structures of ideal crystalline solids. Hence, the principal criticism of cell theories is that they are better suited for modeling crystals than fluid phases.

To address this deficiency, Somer and Kovac[31,32] developed a *variable-structure* cell theory. In this type of model, there are a number of different cell types representing the various local environments of irregularly packed condensed phases. This idea resembles that of the "fluctuating cell" model of Hoover et al.,[33] which has recently been extended[34,35] to treat substances that freeze into plastic crystalline phases.

The variable-structure cell approach is well suited for our purposes because it can treat fluids with complex local structures such as water. The structural complexity of water arises because the geometric constraints of its hydrogen-bond networks limit both the orientations and the coordination numbers of the participating molecules.[36,37] The microscopic picture that has emerged[6,38,39] from both computer simulations[6,39−44] and experiments[45,46] is that hydrogen-bond networks render liquid water locally heterogeneous, with fluctuations between predominantly two types of local environments, (1) structured (lower density) and (2) unstructured (higher density) regions, depending on both temperature and pressure.[47]

C. Theory for the Liquid and Vapor Phases. Our model system consists of *N* identical molecules of diameter *d*. These molecules are contained within *N* neighborhoods that we call "cells". The cells are indistinguishable from each other and fluctuate between states with different structures, volumes, and energies. At a given instant, each cell can be classified as one of three allowable types, (1) *cage-like*, (2) *dense*, or (3) *expanded*, that describe the mutual interaction of a central molecule (labeled B in Figure 2) and two of its neighbors (A and C). The cage-like and dense cell types correspond roughly to the transient structured and unstructured regions observed in computer simulations[6,39−44] and experiments[45,46] of liquid water, and the expanded cell type accounts for the local density fluctuations that give rise to the vapor phase.

We aim to predict the populations $f_j(T,P)$ ($j = 1-3$) of the cell types 1 (cage-like), 2 (dense), and 3 (expanded). The sum of these populations obeys the normalization condition

$$\sum_{j=1}^{3} f_j = 1 \qquad (1)$$

Figure 2 shows a key construct of this model, a *house-shaped* structure that characterizes the local "volume" that is associated with each cell. (We use the term volume instead of area here to maintain the analogy with three-dimensional water. The quantity we calculate is the area of the house.) The sectors of A, B, and C that are contained within one house (shaded region, Figure 2) sum exactly to the volume of one molecule $\pi d^2/4$. The volumes of the N cells sum to the total system volume Nv.

Cage-like Cells, Type 1. Cell type 1 (Figure 2) is a low-energy, cage-like triplet structure in which molecule B can rotate subject to two constraints. First, B is constrained to maintain a perfect hydrogen bond with C (i.e., B and C are in contact and their bonding arms are collinear). Second, molecule A contacts B with its bonding arm pointed toward B's center. The potential energy of this cell u_1 has a square-law dependence on the angle θ that describes the local orientation of molecule B:

$$u_1 = \begin{cases} -\epsilon_{HB} + k_s(\theta - 2\pi/3)^2 & \pi/3 < \theta < \pi \\ -\epsilon_{HB} + k_s(\theta - 4\pi/3)^2 & \pi < \theta < 5\pi/3 \\ \infty & \text{otherwise} \end{cases} \quad (2)$$

where k_s represents the orientational "spring constant" associated with bending the A−B bond, and $-\epsilon_{HB}$ is the energy of the cell's ground-state configuration in which two perfect hydrogen bonds are formed. B cannot access orientations $0 < \theta < \pi/3$ or $5\pi/3 < \theta < 2\pi$ because of the steric repulsions between C and A. The cell volume v_1 of the cage-like structure is

$$v_1(\theta) = a_1(\theta)d^2 \quad (3)$$

where $a_1(\theta) = \sin(\theta/2)[1 + |\cos(\theta/2)|]$. Equation 3 is the sum of two contributions to the house: $d^2 \sin(\theta/2)$ is the volume of the rectangular base and $d^2 \sin(\theta/2)|\cos(\theta/2)|$ is the volume of the triangular roof. Although this volume depends on θ, we assume that the hydrogen bond is sufficiently stiff (i.e., k_s is sufficiently large) that the cell volume can be approximated as the ground-state value,[48]

$$v_1 \approx \frac{3\sqrt{3}d^2}{4} \quad (4)$$

Dense Cells, Type 2. Cell type 2 (Figure 2) is compact: molecules A, B, and C are compressed into mutual contact. This structure has van der Waals contacts, but molecule B does not participate in hydrogen bonds with A or C. The cell interaction energy u_2 and volume v_2 are assumed to be constant, independent of B's orientation:

$$u_2 = -\epsilon_d \quad (5)$$

and

$$v_2 = a_2 d^2 \quad (6)$$

where $a_2 = (2 + \sqrt{3})/4$. Here, $d^2/2$ is the volume of the rectangular base and $\sqrt{3}d^2/4$ is the volume of the triangular roof.

Expanded Cells, Type 3. In this cell type (low local density) (Figure 2), molecule B does not interact with neighbors A and C (aside from the hard-core overlap constraints),

$$u_3 = 0 \quad (7)$$

We approximate the distribution of volumes of the expanded cell by the average volume of a one-dimensional excluded volume gas v_3 (see section below on Statistical Mechanics),

$$v_3 = \frac{k_B T}{P} + b \quad (8)$$

where we choose $b = v_2 = (2 + \sqrt{3})d^2/4$ to be the minimal cell size in the fluid.

Statistical Mechanics. We develop the equilibrium statistical mechanics of this model within the isothermal−isobaric ensemble (constant N, P, and T). We treat the cells in the fluid states as N indistinguishable, weakly interacting (i.e., independent) subsystems, so we express the partition function of the fluid $\Delta(N,P,T)$ as

$$\Delta = \frac{1}{N!}[\Delta_{cell}]^N \quad (9)$$

Δ_{cell} is the partition function for molecule B in its cell, given by

$$\Delta_{cell} = c(T)N\sum_{k=1}^{3}\int\int_{\{k\}} dx\, dy \int_0^{2\pi} d\theta \exp(-[u_k + Pv_k]/k_B T) \quad (10)$$

where k_B is Boltzmann's constant and $c(T)$ is the 2D momentum contribution.[49] The sum is taken over the three cell types (cage-like, dense, and expanded), and (x, y) are the Cartesian coordinates of molecule B (i.e., the central molecule). The double integral $\int\int_{\{k\}} dx\, dy$ represents the translational volume that is accessible to molecule B in cell type k.

This approach, which is similar to that of traditional cell theories, assumes that the degrees of freedom associated with other molecules in the cell (A and C) have been accounted for elsewhere; i.e., molecule A of one cell is the central molecule (B) of another cell. Although approximate, this ensures that the system retains the appropriate $3N$ degrees of freedom ($2N$ translational and N orientational in 2D). The multiplicative factor N in eq 10 accounts for the fact that each of the N molecules in the fluid can be the central molecule of each cell (i.e., the fluid has communal entropy).[28]

To determine Δ_{cell}, we sum over the three cell types:

$$\Delta_{cell} = c(T)N\left\{\exp\left[-\frac{Pv_1}{k_B T}\right]\int\int_{\{1\}} dx\, dy \int_0^{2\pi} d\theta \exp\left[-\frac{u_1(\theta)}{k_B T}\right] + \exp\left[-\frac{Pv_2}{k_B T}\right]\int\int_{\{2\}} dx\, dy \int_0^{2\pi} d\theta \exp\left[-\frac{u_2}{k_B T}\right] + \exp\left[-\frac{Pv_3}{k_B T}\right]\int\int_{\{3\}} dx\, dy \int_0^{2\pi} d\theta \exp\left[-\frac{u_3}{k_B T}\right]\right\} \quad (11)$$

The free volume of molecule B, $\int\int_{\{k\}} dx\, dy$, is a complex function of the locations of all of its neighbors, and thus its determination is beyond the scope of our triplet cell model. We

use the following simple approximation. When molecule B is hydrogen-bonded to, or in van der Waals contact with, molecules A and C (i.e., when it is in either cell type 1 or 2), it is restricted to a molecular-sized free volume $\int\int_{\{1\}} dx\, dy = \int\int_{\{2\}} dx\, dy = d^2$. We assume that it can translate within this local free volume without affecting its energy. Substituting this free volume approximation into the first term in eq 11 and integrating over θ gives

$$\int\int_{\{1\}} dx\, dy \int_0^{2\pi} d\theta \exp\left[-\frac{u_1(\theta)}{k_BT}\right] = d^2 \int_0^{2\pi} d\theta \exp\left[-\frac{u_1(\theta)}{k_BT}\right] = d^2 \exp\left[\frac{\epsilon_{HB}}{k_BT}\right]\left\{\int_{\pi/3}^{\pi} d\theta \exp\left[-\frac{k_s(\theta - 2\pi/3)^2}{k_BT}\right] + \int_{\pi}^{5\pi/3} d\theta \exp\left[-\frac{k_s(\theta - 4\pi/3)^2}{k_BT}\right]\right\} = 2\pi d^2 \exp\left[\frac{\epsilon_{HB}}{k_BT}\right]\sqrt{\frac{k_BT}{\pi k_s}}\,\mathrm{erf}\left(\sqrt{\frac{k_s\pi^2}{9k_BT}}\right) \quad (12)$$

Similarly, for cell type 2 we get

$$\int\int_{\{2\}} dx\, dy \int_0^{2\pi} d\theta \exp\left[-\frac{u_2}{k_BT}\right] = d^2 \int_0^{2\pi} d\theta \exp\left[\frac{\epsilon_d}{k_BT}\right] = 2\pi d^2 \exp\left[\frac{\epsilon_d}{k_BT}\right] \quad (13)$$

In the expanded cell (type 3), molecule B is no longer constrained to be in contact with A or C. We assume that its free volume can now be described by the simple excluded-volume expression $\int\int_{\{3\}} dx\, dy = v_3 - b$, which gives

$$\int\int_{\{3\}} dx\, dy \int_0^{2\pi} d\theta \exp\left[-\frac{u_3}{k_BT}\right] = (v_3 - b)\int_0^{2\pi} d\theta \exp\left[-\frac{u_3}{k_BT}\right] = 2\pi(v_3 - b) \quad (14)$$

where $b = v_2 = (2 + \sqrt{3})d^2/4$ is the excluded volume parameter that appears in van der Waals theories. Substituting eqs 12−14 into eq 11 gives the partition function for molecule B in its fluctuating cell Δ_{cell}

$$\Delta_{cell} = 2\pi d^2 c(T) N\left\{\exp\left[\frac{-Pv_1 + \epsilon_{HB}}{k_BT}\right]\sqrt{\frac{k_BT}{k_s\pi}}\,\mathrm{erf}\left(\sqrt{\frac{k_s\pi^2}{9k_BT}}\right) + \exp\left[\frac{-Pv_2 + \epsilon_d}{k_BT}\right] + \exp\left[\frac{-Pv_3}{k_BT}\right]\frac{(v_3 - b)}{d^2}\right\} \quad (15)$$

It can be shown that $v_3 = (k_BT/P) + b$ (given by eq 8) can also be derived by maximizing Δ_{cell} in eq 15 with respect to v_3 at constant N, P, and T (i.e., finding the value of v_3 that satisfies $[\partial\Delta_{cell}/\partial v_3]_{NPT} = 0$ and $[\partial^2\Delta_{cell}/\partial v_3^2]_{NPT} < 0$).

Now, to simplify later results, we rewrite Δ_{cell} in terms of average energies $\langle u_j\rangle$ and corresponding densities of states g_j for the three energy levels $j = 1-3$. The average energies are

$$\langle u_1\rangle = \frac{\int_0^{2\pi} d\theta u_1(\theta)\exp[-u_1(\theta)/k_BT]}{\int_0^{2\pi} d\theta \exp[-u_1(\theta)/k_BT]} = -\epsilon_{HB} + k_s\frac{\int_{\pi/3}^{\pi} d\theta\,(\theta - 2\pi/3)^2 e^{-k_s(\theta-2\pi/3)^2/k_BT} + \int_{\pi}^{5\pi/3} d\theta\,(\theta - 4\pi/3)^2 e^{-k_s(\theta-4\pi/3)^2/k_BT}}{\int_{\pi/3}^{\pi} d\theta\, e^{-k_s(\theta-2\pi/3)^2/k_BT} + \int_{\pi}^{5\pi/3} d\theta\, e^{-k_s(\theta-4\pi/3)^2/k_BT}} = -\epsilon_{HB} + \frac{\sqrt{\pi/k_s}(k_BT)^{3/2}\,\mathrm{erf}(\sqrt{k_s\pi^2/9k_BT}) - (2/3)\pi k_BT\exp(-k_s\pi^2/9k_BT)}{2\sqrt{\pi k_BT/k_s}\,\mathrm{erf}(\sqrt{k_s\pi^2/9k_BT})} = -\epsilon_{HB} + \frac{k_BT}{2} - \sqrt{k_s\pi k_BT}\frac{\exp(-k_s\pi^2/9k_BT)}{3\,\mathrm{erf}(\sqrt{k_s\pi^2/9k_BT})}$$

$$\langle u_2\rangle = \frac{\int_0^{2\pi} d\theta u_2 \exp[-u_2/k_BT]}{\int_0^{2\pi} d\theta \exp[-u_2/k_BT]} = u_2 = -\epsilon_d$$

$$\langle u_3\rangle = \frac{\int_0^{2\pi} d\theta u_3 \exp[-u_3/k_BT]}{\int_0^{2\pi} d\theta \exp[-u_3/k_BT]} = u_3 = 0 \quad (16)$$

The relations given in eq 16 can be used to eliminate the energetic parameters ϵ_{HB} and ϵ_d from eq 15, yielding the following expression for Δ_{cell}

$$\Delta_{cell} = \frac{N}{e}\sum_{j=1}^{3} g_j \exp[-(\langle u_j\rangle + Pv_j)/k_BT] \equiv \frac{N}{e}\sum_{j=1}^{3}\Delta_j \quad (17)$$

where the rightmost equality in eq 17 defines Δ_j. The prefactors g_1, g_2, and g_3 that result from this conversion to average energies give the densities of states of the cell types:

$$g_1(T) = 2\pi d^2 c(T) e\frac{\mathrm{erf}(\sqrt{k_s\pi^2/9k_BT})}{\sqrt{k_s\pi/k_BT}} \times \exp\left(\frac{1}{2} - \frac{\sqrt{k_s\pi/k_BT}\exp[-k_s\pi^2/9k_BT]}{3\,\mathrm{erf}(\sqrt{k_s\pi^2/9k_BT})}\right)$$

$$g_2(T) = 2\pi d^2 c(T) e$$

$$g_3(T,P) = 2\pi c(T) e(v_3 - b) = 2\pi c(T) e\frac{k_BT}{P} \quad (18)$$

The fractional populations of the cell types $f_j(T,P)$ are obtained from eq 17,

$$f_j = \frac{g_j \exp[-(\langle u_j\rangle + Pv_j)/k_BT]}{\sum_{k=1}^{3} g_k \exp[-(\langle u_k\rangle + Pv_k)/k_BT]} = \frac{\Delta_j}{\sum_k \Delta_k} \quad (19)$$

These populations are the fundamental microscopic quantities in the model.

Finally, substituting eq 17 into eq 9 and applying Stirling's approximation $N! \simeq (N/e)^N$ leads to a very simple form for the partition function of the fluid:

$$\Delta = \frac{1}{N!}[\Delta_{cell}]^N = (\sum_{j=1}^{3}\Delta_j)^N \quad (20)$$

Our model differs substantially from conventional cell theories[28−30] that focus on a central molecule surrounded by a static first shell of nearest neighbors. Our cells describe only

molecular triplets, not whole cages, and the cell populations depend on temperature and pressure. For example, increasing the pressure can shift the cell population from cage-like cells to dense cells. That is, a cell around a central molecule B can change structure. Moreover, our central molecule B is not confined to remain in one cell. Instead, each of the N molecules can be the central molecule of any cell (i.e., the molecules are not localized in space), giving rise to a *communal* contribution to the fluid's entropy that is not present in the crystalline phases.[28]

Computing Macroscopic Properties from the Partition Function. The chemical potential μ of the fluid can be obtained directly from the partition function Δ given in eq 20

$$\mu = -k_B T \frac{\ln \Delta}{N} = -k_B T \ln\{\sum_{j=1}^{3} \Delta_j\} \tag{21}$$

The molar volume $v(T,P)$, i.e., the equation of state of the fluid, comes from differentiating μ with respect to P,

$$\begin{aligned} v &= \left[\frac{\partial \mu}{\partial P}\right]_T = -\frac{k_B T}{N\Delta}\left[\frac{\partial \Delta}{\partial P}\right]_T \\ &= \frac{v_1\Delta_1 + v_2\Delta_2 + \left(\frac{k_B T}{P} + b\right)\Delta_3}{\sum_{k=1}^{3}\Delta_k} = \frac{\sum_{j=1}^{3} v_j \Delta_j}{\sum_{k=1}^{3}\Delta_k} \\ &= \sum_{j=1}^{3} f_j v_j \end{aligned} \tag{22}$$

where the f_j are given by eq 19. Similarly, the molar enthalpy h is given by

$$\begin{aligned} h &= \mu + Ts = \mu - T\left[\frac{\partial \mu}{\partial T}\right]_P \\ &= \frac{k_B T^2 \sum_{j=1}^{3} (\partial \Delta_j/\partial T)_P}{\sum_{k=1}^{3}\Delta_k} = \frac{\sum_{j=1}^{3} (3k_B T/2 + \langle u_j\rangle + P v_j)\,\Delta_j}{\sum_{k=1}^{3}\Delta_k} \\ &= \sum_{j=1}^{3} f_j h_j \end{aligned} \tag{23}$$

where h_j is the enthalpy of cell type j

$$h_j = e_j + P v_j \tag{24}$$

and $e_j = 3k_B T/2 + \langle u_j\rangle$ is its energy. The enthalpy of the fluid h, like its volume v, is a linear combination of contributions from each cell type. From these relations, we obtain the other thermodynamic quantities: the molar entropy s,

$$s = [h - \mu]/T = \sum_j f_j h_j/T + k_B \ln\{\sum_{j=1}^{3}\Delta_j\} \tag{25}$$

the isobaric heat capacity c_P,

$$c_P = \left[\frac{\partial h}{\partial T}\right]_P = \sum_{j=1}^{3} f_j h_j \left\{\left[\frac{\partial \ln f_j}{\partial T}\right]_P + \left[\frac{\partial \ln h_j}{\partial T}\right]_P\right\} \equiv \sum_{j=1}^{3} c_{P,j} \tag{26}$$

the isothermal compressibility κ_T,

$$\kappa_T = -\left[\frac{\partial \ln v}{\partial P}\right]_T = -\frac{1}{v}\sum_{j=1}^{3} f_j v_j \left\{\left[\frac{\partial \ln f_j}{\partial P}\right]_T + \left[\frac{\partial \ln v_j}{\partial P}\right]_T\right\} \equiv \sum_{j=1}^{3} \kappa_{T,j} \tag{27}$$

and the thermal expansion coefficient α_P,

$$\alpha_P = \left[\frac{\partial \ln v}{\partial T}\right]_P = \frac{1}{v}\sum_{j=1}^{3} f_j v_j \left\{\left[\frac{\partial \ln f_j}{\partial T}\right]_P + \left[\frac{\partial \ln v_j}{\partial T}\right]_P\right\} \equiv \sum_{j=1}^{3} \alpha_{P,j} \tag{28}$$

Each of the thermodynamic response functions, c_P, α_P, and κ_T, involves two temperature- and pressure-dependent contributions from each cell type, arising from (1) changes in its population f_j and (2) changes in its properties (i.e., h_j or v_j) (see also Appendix A).

Cell−Cell Attractions. So far, we have neglected interactions between one cell and another. We now account approximately for these interactions. We assume that neighboring cells interact through an orientation-independent van der Waals attraction. Hence, we add a van der Waals term $-Na/v$ to the average energy, where a is a constant and v is the equilibrium molar volume. Because this dispersion energy does not affect local molecular structuring, it can readily be incorporated into the theory self-consistently[50] as follows. As is shown in Appendix B, "turning on" a uniform attractive potential $-Na/v$ (at constant N, V, and T) in a generic system reduces its pressure from P_0 to $P = P_0 - a/v^2$, as in the van der Waals or Bragg−Williams theories. Therefore, to determine the molar volume v at pressure P for nonzero a, we simply evaluate[50] eq 22 at the larger pressure P_0.

$$\begin{aligned} v &= f_1(T,P_0)v_1 + f_2(T,P_0)v_2 + f_3(T,P_0)\, v_3(T,P_0) \\ &= \sum_{j=1}^{3} f_{j,0} v_{j,0} = v_0 \end{aligned} \tag{29}$$

where P_0 satisfies the identity

$$P_0 = P + a/{v_0}^2 \tag{30}$$

Throughout this section the subscript "0" is used to indicate that a function is evaluated at P_0 given in eq 30, e.g., $v_0 \equiv v(T,P_0)$. Note that, from eq 29, the mean-field adjusted fractional populations at pressure P are now given by $f_j = f_{j,0}$. The chemical potential μ at pressure P and nonzero a can be determined by evaluating eq 21 at P_0 and adding the van der Waals contribution $-2a/v_0$ (see Appendix B):

$$\mu = \mu_0 - 2a/v_0 \tag{31}$$

The effects of the dispersion field on other thermodynamic functions follow from eqs 29−31. For example, we get the molar enthalpy h,

$$h = \mu + Ts = \mu - T\left[\frac{\partial \mu}{\partial T}\right]_P = h_0 - 2a/v_0 \tag{32}$$

the molar entropy s,

$$s = [h - \mu]/T = s_0 \tag{33}$$

the isothermal compressibility κ_T,

$$\kappa_T = \sum_{j=1}^{3} \kappa_{T,j} = -\sum_{j=1}^{3} \frac{1}{v_0}\left(\frac{\partial f_{j,0} v_{j,0}}{\partial P}\right)_T = \frac{\kappa_{T,0}}{1 - 2a\kappa_{T,0}/{v_0}^2} \quad (34)$$

the thermal expansion coefficient α_P,

$$\alpha_P = \sum_{j=1}^{3} \alpha_{P,j} = \sum_{j=1}^{3} \frac{1}{v_0}\left(\frac{\partial f_{j,0} v_{j,0}}{\partial T}\right)_P = \frac{\alpha_{P,0}}{1 - 2a\kappa_{T,0}/{v_0}^2} \quad (35)$$

and the isobaric heat capacity c_P,

$$c_P = \sum_{j=1}^{3} c_{P,j} = \sum_{j=1}^{3} \left[\frac{\partial f_{j,0}(h_{j,0} - 2a/v_0)}{\partial T}\right]_P = c_{P,0} + \frac{2aT{\alpha_{P,0}}^2}{v_0\{1 - 2a\kappa_{T,0}/{v_0}^2\}} \quad (36)$$

The results presented in eqs 29−36 are used in section III to calculate the physical properties of the fluid phases.

In the high-temperature limit $T \to \infty$, the system is dominated by cell type 3 ($f_1 \to 0$, $f_2 \to 0$, $f_3 \to 1$), and our model equation of state becomes identical to that of a 2D van der Waals fluid

$$\underset{T\to\infty}{P} \to \frac{k_B T}{v - b} - \frac{a}{v^2} \quad (37)$$

Our aim in the following sections is to develop an analytical model of the phase diagram. Computing the phase diagram requires knowledge of the possible crystalline phases. Liquid−solid phase transitions have been modeled successfully by cell theories[34,35,51−54] and other statistical mechanical approaches.[55] In those simple strategies, the solid states are not predicted by the model; they are assumed as inputs. Water has at least 12 distinct crystalline phases[56] under various conditions of temperature and pressure, and although there has been progress in this regard, modeling these solid phases has been quite challenging even with microscopically detailed potentials.[57]

D. Theory for the Crystalline Phases. What are the crystalline phases of the present model? As a first step, we consider two types of crystalline phases: a low-pressure (LP) ice and a high-pressure (HP) ice. Our choice for the LP phase is simplified by the fact that there is only one possible crystalline arrangement that permits the maximum number of perfect hydrogen bonds per molecule. This low-density crystal structure, shown in Figure 3a, is analogous to hexagonal ice I_h, and it is also the crystalline phase that has been observed in low-temperature Monte Carlo simulations of the MB model.[21]

Water also has denser forms of ice at high pressures. To explore the possible structures of a dense crystalline phase, we recall that there is a unique minimum-volume ($v = \sqrt{3}d^2/2$) arrangement for 2D disks in the plane. Figure 3b illustrates one candidate structure, which we call the HP crystal, that conforms to this triangular packing arrangement.

The two ices described above do not exhaust the possible crystalline structures for this model. However, a preliminary search using the theory outlined below has not revealed other stable crystals. Hence, we take the model's LP and the HP phases as being representative of water's crystalline forms.

Model of LP Ice. The LP ice structure shown in Figure 3a can be divided into N cells, each containing one molecule

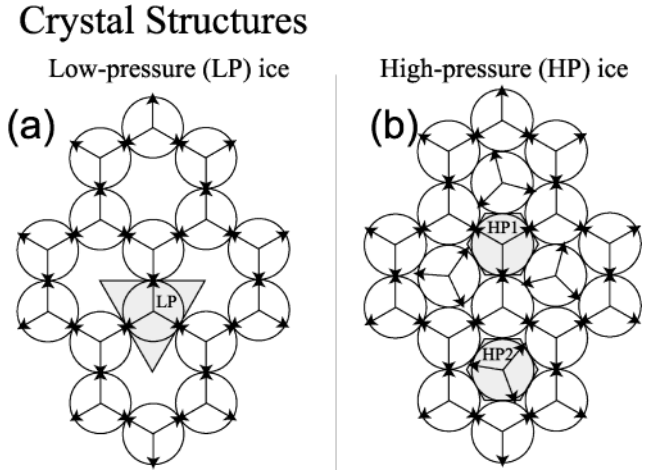

Figure 3. (a) Structure of low-pressure (LP) ice. (b) Structure of high-pressure (HP) ice.

bonded to its three nearest neighbors. These triangular cells contain all points in space that are closer to the central molecule than to any other molecule in the system; i.e., they are the *Voronoi polygons*[58] associated with each molecule. As in traditional cell theories, the three neighboring molecules are fixed in their ground-state positions and orientations, whereas the central molecule can rotate. We assume spring-like angular fluctuations of the central molecule with respect to its perfectly hydrogen-bonded cage (as measured by angle θ), so the potential energy of this cell u_{LP} is

$$u_{LP}(\theta) = \begin{cases} -3\epsilon_{HB}/2 + 3k_s\theta^2 & 0 < \theta < \pi/3 \\ -3\epsilon_{HB}/2 + 3k_s(\theta - 2\pi/3)^2 & \pi/3 < \theta < \pi \\ -3\epsilon_{HB}/2 + 3k_s(\theta - 4\pi/3)^2 & \pi < \theta < 5\pi/3 \\ -3\epsilon_{HB}/2 + 3k_s(\theta - 2\pi)^2 & 5\pi/3 < \theta < 2\pi \end{cases} \quad (38)$$

and its volume v_{LP} is given by

$$v_{LP} = \frac{3\sqrt{3}}{4}d^2 \quad (39)$$

Because the ground-state involves three hydrogen bonds, the ground-state energy of the central molecule is $-3\epsilon_{HB}/2$. Its torsional spring constant is $3k_s$, three times the value associated with bending one hydrogen bond in the cage-like cell type 1 of the liquid.

The isothermal−isobaric partition function for the crystal Δ is given by

$$\Delta = \exp(-N\mu/k_B T) = [\Delta_{cell}]^N \quad (40)$$

This expression is identical to that of the fluid (eq 9) except without the factor of $N!$ in the denominator, because the molecules are localized (and thus distinguishable) in the crystal. We express Δ_{cell} as follows:

$$\Delta_{cell} = c(T)\int d\theta \exp(-[u_{LP}(\theta) + Pv_{LP}]/k_B T) \quad (41)$$

As in the fluid phases, x and y describe the position of the central molecule. In eq 41, we have assumed incompressibility, $v(T,P) = v_{LP}$. Also, as in the cage-like (type 1) and dense (type 2) cells of the liquid in eqs 12 and 13, we simply replace the double integral over the allowable positions with the molecular-size free volume $\int\int_{\{LP\}} dx\, dy = d^2$. Substituting $u_{LP}(\theta)$ into eq 41

and performing the integration leads to

$$\Delta_{\text{cell}} = c(T)\exp[-P\upsilon_{\text{LP}}/k_{\text{B}}T]\int\int_{\{\text{LP}\}} \mathrm{d}x\,\mathrm{d}y \times \int_0^{2\pi} \mathrm{d}\theta \exp[-u_{\text{LP}}(\theta)/k_{\text{B}}T]$$

$$= d^2c(T)\exp[-P\upsilon_{\text{LP}}/k_{\text{B}}T]\exp[3\epsilon_{\text{HB}}/2k_{\text{B}}T] \times \{\int_{-\pi/3}^{\pi/3} \mathrm{d}\theta\, \mathrm{e}^{-3k_s\theta^2/k_{\text{B}}T} + \int_{\pi/3}^{\pi} \mathrm{d}\theta\, \mathrm{e}^{-3k_s(\theta-2\pi/3)^2/k_{\text{B}}T} + \int_{\pi}^{5\pi/3} \mathrm{d}\theta\, \mathrm{e}^{-3k_s(\theta-4\pi/3)^2/k_{\text{B}}T}\}$$

$$= 2\pi d^2c(T)\exp\left[\frac{3\epsilon_{\text{HB}}/2 - P\upsilon_{\text{LP}}}{k_{\text{B}}T}\right]\frac{3\,\mathrm{erf}(\sqrt{k_s\pi^2/3k_{\text{B}}T})}{2\sqrt{3k_s\pi/k_{\text{B}}T}} \quad (42)$$

Substituting eq 42 into eq 40 yields the chemical potential μ

$$\mu = -k_{\text{B}}T\ln\{g_{\text{LP}}\exp[-(\langle u_{\text{LP}}\rangle + P\upsilon_{\text{LP}})/k_{\text{B}}T]\} \quad (43)$$

As before, we use the average cell energy $\langle u_{\text{LP}}\rangle$,

$$\langle u_{\text{LP}}\rangle = \frac{\int_0^{2\pi} \mathrm{d}\theta\, u_{\text{LP}}(\theta)\exp[-u_{\text{LP}}(\theta)/k_{\text{B}}T]}{\int_0^{2\pi} \mathrm{d}\theta \exp[-u_{\text{LP}}(\theta)/k_{\text{B}}T]}$$

$$= -\frac{3\epsilon_{\text{HB}}}{2} + \frac{k_{\text{B}}T}{2} - \sqrt{3k_s\pi k_{\text{B}}T}\frac{\exp(-k_s\pi^2/3k_{\text{B}}T)}{3\,\mathrm{erf}(\sqrt{k_s\pi^2/3k_{\text{B}}T})} \quad (44)$$

and the corresponding density of states g_{LP},

$$g_{\text{LP}} = 2\pi d^2c(T)\frac{3\,\mathrm{erf}(\sqrt{k_s\pi^2/3k_{\text{B}}T})}{2\sqrt{3k_s\pi/k_{\text{B}}T}} \times \exp\left(\frac{1}{2} - \frac{\sqrt{3k_s\pi/k_{\text{B}}T}\exp[-k_s\pi^2/3k_{\text{B}}T]}{3\,\mathrm{erf}(\sqrt{k_s\pi^2/3k_{\text{B}}T})}\right) \quad (45)$$

Equation 43 holds only for cases where the dispersion term vanishes, i.e., $a = 0$. As in the fluid, to calculate the chemical potential μ for nonzero a, we make the substitution

$$\mu(T,P) = \mu\left(T, P + \frac{a}{[\upsilon_{\text{LP}}]^2}\right) - 2a/\upsilon_{\text{LP}} \quad (46)$$

Model of HP Ice. Our model of HP ice is shown in Figure 3b. In short, HP ice is simply LP ice with the interior of each hexagonal cage filled by a water molecule. So HP ice has two cell types. Two-thirds of the molecules form a lattice that is identical to the hexagonal cages of the LP phase. The molecules in the other one-third are the internal free waters. We refer to the former as HP cells of type 1 (HP1) and the latter as HP cells of type 2 (HP2).

We take the potential energy of HP1 u_{HP1} to be identical to the LP cell given by eq 38:

$$u_{\text{HP1}}(\theta) = u_{\text{LP}}(\theta) \quad (47)$$

We assume the potential energy of HP2 u_{HP2} is zero,

$$u_{\text{HP2}}(\theta) = 0 \qquad 0 \le \theta \le 2\pi \quad (48)$$

Because the cells are independent and distinguishable, the isothermal−isobaric partition function Δ is given by a product of the component cell quantities:

$$\Delta = \exp(-N\mu/k_{\text{B}}T) = [\Delta_{\text{cell,HP1}}]^{2N/3}[\Delta_{\text{cell,HP2}}]^{N/3} \quad (49)$$

Following a development similar to that of eqs 41−45, the chemical potential of HP ice can be shown to be given by

$$\mu = -\frac{2}{3}k_{\text{B}}T\ln\{g_{\text{HP1}}\exp[-(\langle u_{\text{HP1}}\rangle + P\upsilon_{\text{HP1}})/k_{\text{B}}T]\} - \frac{1}{3}k_{\text{B}}T\ln\{g_{\text{HP2}}\exp[-(\langle u_{\text{HP2}}\rangle + P\upsilon_{\text{HP2}})/k_{\text{B}}T]\} \quad (50)$$

where $\langle u_{\text{HP1}}\rangle = \langle u_{\text{LP}}\rangle$ given by eq 44, $g_{\text{HP1}} = g_{\text{LP}}$ given by eq 45, $\upsilon_{\text{HP1}} = \upsilon_{\text{HP2}} = \sqrt{3}\,d^2/2$, $\langle u_{\text{HP2}}\rangle = 0$, and $g_{\text{HP2}} = 2\pi d^2c(T)$.

As before, eq 50 holds only when $a = 0$. Again, to calculate the chemical potential $\mu(T,P)$ for nonzero a, we make the substitution

$$\mu(T,P) = \mu\left(T, P + \frac{a}{[\upsilon_{\text{HP1}}]^2}\right) - 2a/\upsilon_{\text{HP1}} \quad (51)$$

TABLE 1: Reduced Thermodynamic Variables[a]

temperature	$T_{\text{r}} = T/T_{\text{C}}$
pressure	$P_{\text{r}} = P/P_C$
volume	$\upsilon_{\text{r}} = V/V_{\text{C}}$
isothermal compressibility	$\kappa_T^* \equiv -(\partial \ln \upsilon_{\text{r}}/\partial P_{\text{r}})_{T_{\text{r}}} = \kappa_T P_{\text{C}}$
thermal expansion coefficient	$\alpha_P^* \equiv (\partial \ln \upsilon_{\text{r}}/\partial T_{\text{r}})_{P_{\text{r}}} = \alpha_P T_{\text{C}}$

[a] The subscript C indicates that the quantity is evaluated at the liquid−vapor critical point.

III. Comparison with Experiments and Molecular Simulations

A. Phase Diagram. We now explore the phase diagram of the model. To compare with experimental data, we use the reduced thermodynamic variables shown in Table 1. In this representation, the results depend on three parameters: $a/(d^2\epsilon_{\text{HB}})$, $\epsilon_{\text{d}}/\epsilon_{\text{HB}}$, and k_s/ϵ_{HB}. These dimensionless combinations quantify the ratios of the characteristic dispersion energy a/d^2, the dense state energy ϵ_{d}, and the bonding spring constant k_s to the characteristic hydrogen-bonding energy ϵ_{HB}.

Figure 4 compares the phase behavior of the model to the experimental phase diagram for water. The curves locate the phase boundaries in the pressure−temperature plane. These boundaries are calculated by determining, for each temperature T, the pressure P at which the chemical potentials of two competing phases are equal.[59] The parameters used to calculate the theoretical phase diagram are shown in Table 2. Although this parameter set has not been optimized to match any particular property of water, it was found to yield a good overall description of the experimental data.

The theory reproduces many of the distinguishing features of water's phase diagram. For instance, the melting line for LP ice is negatively sloped in the pressure−temperature plane, indicating that the liquid is denser than LP ice along the coexistence curve. At high pressure, LP ice undergoes a first-order transition to the HP ice, which exhibits a "normal" positively sloped melting line. These phase transitions are qualitatively similar to those involving the experimental low-pressure and high-pressure forms of ice (e.g., ice I_h and ice VII, respectively).[56] The theoretical melting and boiling curves are shown to converge to a liquid−solid−vapor triple point, below which only the vapor or solid states are thermodynamically stable. In agreement with the phase diagram of water, the triple point temperature is roughly 42% of the vapor−liquid critical temperature.

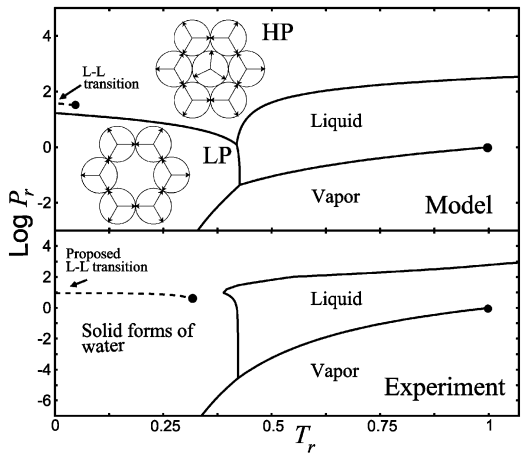

Figure 4. Phase diagrams of water: model (top) and experiments (bottom) in the plane of reduced pressure P_r versus reduced temperature T_r. The unbroken curves are the phase boundaries of the first-order transitions discussed in the text. For clarity, the many solid−solid transitions in the experimental phase diagram of water have been omitted. The dashed curves are the metastable liquid−liquid transitions discussed in the text. See Mishima and Stanley[6] for a discussion of the proposed liquid−liquid phase transition in supercooled water. The values of the parameters used for the theory are given in Table 2.

TABLE 2: Dimensionless Parameters for the Model

$a/d^2\epsilon_{HB}$	0.295
ϵ_d/ϵ_{HB}	0.15
k_s/ϵ_{HB}	100000

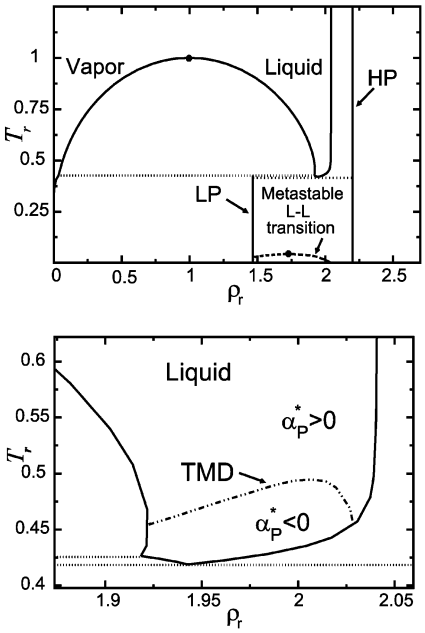

Figure 5. (a) Phase diagram of the model in the plane of reduced temperature T_r versus reduced density ρ_r. The unbroken curves are the phase boundaries of the first-order transitions discussed in the text. The dashed curve is the metastable liquid-liquid transition. The dotted lines connect coexisting densities for the model's two triple points. (b) Detailed view of the liquid state. The dot−dashed curve is the temperature of maximum density (TMD). For temperatures below the TMD, the liquid expands upon isobaric cooling. For temperatures above the TMD, it contracts upon isobaric cooling.

Although the present model predicts first-order freezing transitions, in agreement with experiments, this may be a consequence of our mean-field treatment. The Kosterlitz−Thouless−Halperin−Nelson−Young (KTHNY) theory predicts that topological defects in 2D crystals can cause melting via a continuous transition instead of a first-order transition (see reviews by Strandburg[60] and Glaser and Clark[61]).

Figure 5a shows the model's phase diagram from a different perspective, namely in the reduced temperature−density (T_r, ρ_r) plane, where $\rho_r = 1/v_r$. The coexistence curves are calculated directly from the pressure−temperature phase boundaries shown in Figure 4 using the equations of state of the various phases (see section II). The region of thermodynamic stability for the liquid is bounded above by the vapor−liquid critical temperature and is bounded below by the freezing transitions to the LP and HP phases. A detailed view of this region is shown in Figure 5b. The model correctly predicts that the liquid exhibits a negative thermal expansion coefficient ($\alpha_p^* < 0$), i.e., it expands upon cooling, over a broad range of conditions. The values of temperature and density for which this anomalous behavior occurs are enclosed in Figure 5b by the locus of points that satisfy $\alpha_p^* = 0$ (the temperature of maximum density, TMD).

The theory also addresses an interesting aspect of supercooled water. It predicts a low-temperature liquid−liquid immiscibility, i.e., a first-order phase transition between two structurally distinct deeply supercooled liquid phases (shown in Figure 4): a high-density liquid (with mostly dense triplet structures) and a low-density liquid (with mostly open, cage-like structures). This is consistent with the view that the "first-order" transformation[6,62−64] between water's low-density and high-density glassy forms (LDA and HDA, respectively) is an arrested signature of an underlying liquid−liquid transition[6,40] (Figure 4). We note that vitrification (glass formation) and crystallization (ice formation) in deeply supercooled water have thus far prevented the experimental verification of this hypothesis.[65]

B. Thermodynamic Anomalies of the Liquid State. Figure 6 compares the model's predictions for the reduced molar volume v_r, thermal expansion coefficient α_p^*, isothermal compressibility κ_T^*, and isobaric heat capacity c_P with experimental data for water at atmospheric pressure.[66] The model captures liquid water's distinctive behavior, including negative α_p^* and sharp increases in v_r, κ_T^*, and c_P upon supercooling. It also reproduces qualitatively the discontinuous changes in these quantities across water's first-order freezing transition to hexagonal ice.

C. Structural Basis for the Properties of Water. To explore the microscopic basis for the model's predictions, we examine in Figures 7−13 the behavior of the local cell populations f_j, ($j = 1$) cage-like, ($j = 2$) dense, and ($j = 3$) expanded, and their contributions to various thermodynamic properties. These figures illustrate the entire temperature range of the liquid at atmospheric pressure, from the coldest supercooled state ($T_r = 0$) to the hottest superheated state (the liquid−vapor spinodal temperature, $T_r \approx 0.8025$). Unbroken vertical lines mark the locations of the first-order freezing and boiling transitions. "Stable" indicates the temperature range where the liquid has a lower chemical potential than either the vapor or the crystalline phases. "Supercooled" and "superheated" denote the temperature ranges where the liquid is metastable with respect to LP ice and the vapor, respectively. For comparison, Figure 14 illustrates the experimental behavior of liquid water's thermodynamic response functions in the supercooled region.

Figure 7 shows that the coldest supercooled liquid consists of almost entirely hydrogen-bonded, cage-like structures. As it is heated toward the freezing transition, the orientational constraints of the hydrogen bonds are broken, and the cages "melt" into dense cell types. The stable liquid consists of a

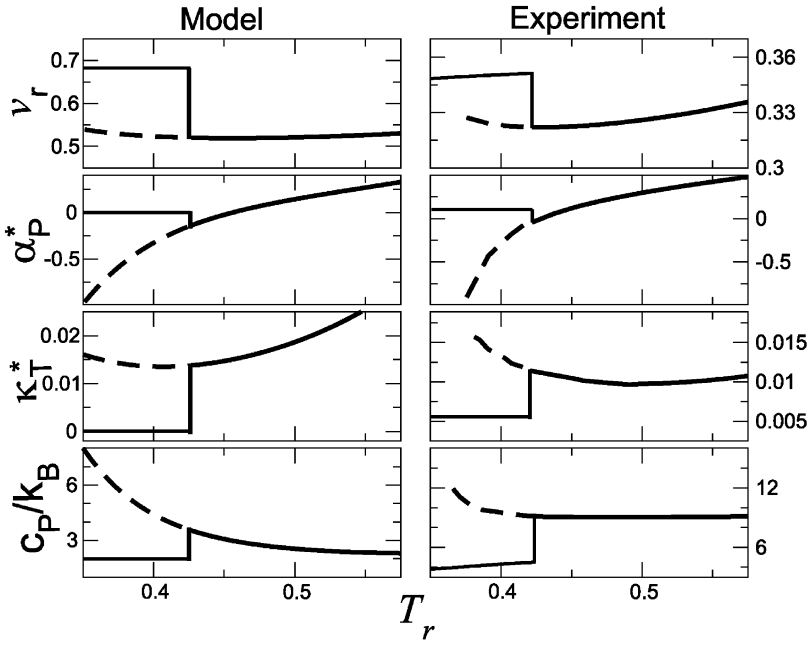

Figure 6. Water's thermodynamic properties versus reduced temperature T_r at atmospheric pressure:[66] model (left) and experiment[84] (right). The solid lines are the properties of the stable liquid and crystalline phases, and the dashed lines are the properties of the supercooled liquid. The discontinuities occur at the first-order freezing transition. (a) Reduced volume v_r, (b) dimensionless thermal expansion coefficient $\alpha_P^* \equiv (\partial \ln v_r/\partial T_r)_{P_r}$, (c) dimensionless isothermal compressibility $\kappa_T^* \equiv -(\partial \ln v_r/\partial P_r)_{T_r}$, and (d) dimensionless isobaric heat capacity c_P/k_B.

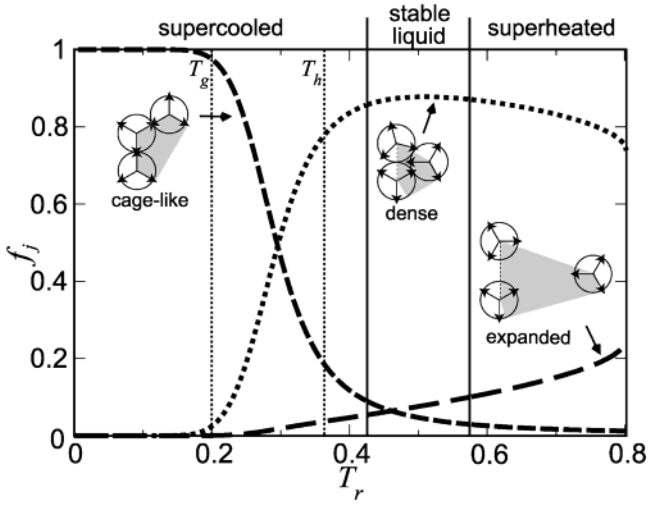

Figure 7. Populations f_j of the ($j = 1$) cage-like, ($j = 2$) dense, and ($j = 3$) expanded cells versus reduced temperature T_r at atmospheric pressure.[66] Recall that $\sum_j f_j = 1$. The unbroken vertical lines are the freezing T_f and boiling T_b temperatures that bound the stable liquid region. The dotted vertical lines labeled T_g and T_h are the experimental[6] glass transition and homogeneous nucleation temperatures for liquid water.

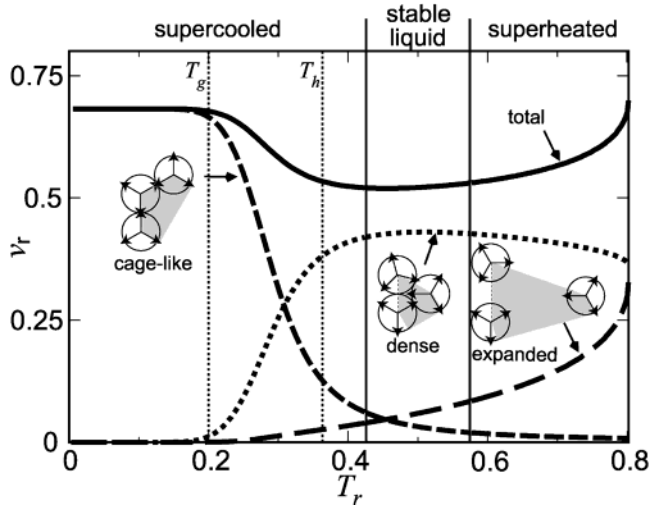

Figure 8. Cell contributions to the liquid's molar volume $f_j v_j/v_C$ from the ($j = 1$) cage-like, ($j = 2$) dense, and ($j = 3$) expanded cell types versus reduced temperature T_r at atmospheric pressure.[66] The unbroken curve is the total molar volume $v_r = \sum_j f_j v_j/v_C$. Other labels are given in Figure 7.

combination of cage-like, dense, and expanded triplet arrangements. In the superheated range, however, the liquid's structure becomes an essentially bimodal distribution of dense and expanded cells, with few hydrogen-bonded states. Note that the populations shown in Figure 7 behave qualitatively similar to (1) water's experimental hydrogen-bond populations as deduced from IR spectroscopic data and (2) water's molecular cluster populations as predicted from ab initio calculations.[17]

The volumetric properties of the liquid are shown in Figure 8. The coldest water is low-density, dominated by open cages. Heating the supercooled liquid increases the density as cages (cell type 1) collapse into dense structures (cell type 2). In the stable liquid range, the balance of properties is subtle. Near the freezing point, heating still predominantly converts cages into dense structures ($1 \rightarrow 2$), increasing the density. However, near boiling, heating converts both cage-like and dense structures into expanded structures ($1, 2 \rightarrow 3$), decreasing the density. The minimum in molar volume occurs at the temperature where there is a balance between these two competing effects.

The theory also offers insights into the model's thermodynamic response functions. As is shown in eqs 35 and 36, α_P and c_P can be expressed as sums of contributions from the cell types, $\alpha_P = \sum_j \alpha_{P,j}$ and $c_P = \sum_j c_{P,j}$. These contributions are plotted in Figures 9 and 10. Figure 9 shows that the negative thermal expansion coefficient in cold and supercooled water results from the collapse of the hydrogen-bond cages, increasing the density with increasing temperature. The positive thermal

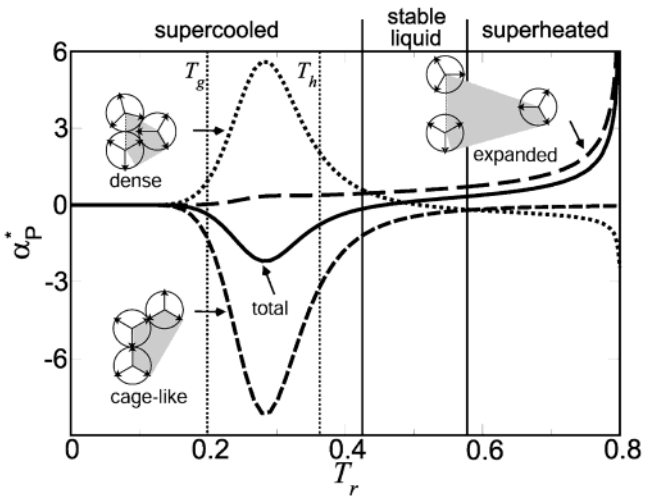

Figure 9. Cell contributions to the liquid's thermal expansion coefficient $\alpha_{P,j}T_C$ from the ($j = 1$) cage-like, ($j = 2$) dense, and ($j = 3$) expanded cell types versus reduced temperature T_r at atmospheric pressure.[66] The unbroken curve is the total thermal expansion coefficient $\alpha_P^* = \sum_j \alpha_{P,j}T_C$. Other labels are given in Figure 7.

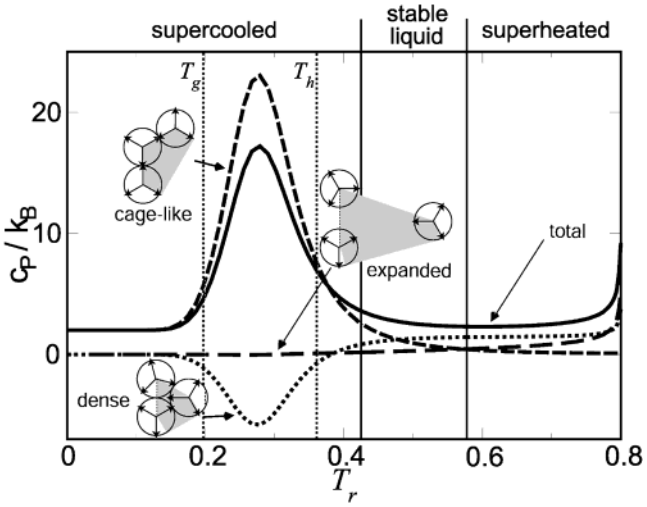

Figure 10. Cell contributions to the liquid's isobaric heat capacity $c_{P,j}/k_B$ from the ($j = 1$) cage-like, ($j = 2$) dense, and ($j = 3$) expanded cell types versus reduced temperature T_r at atmospheric pressure.[66] The unbroken curve is the total isobaric heat capacity $c_P^* = \sum_j c_{P,j}/k_B$. Other labels are given in Figure 7.

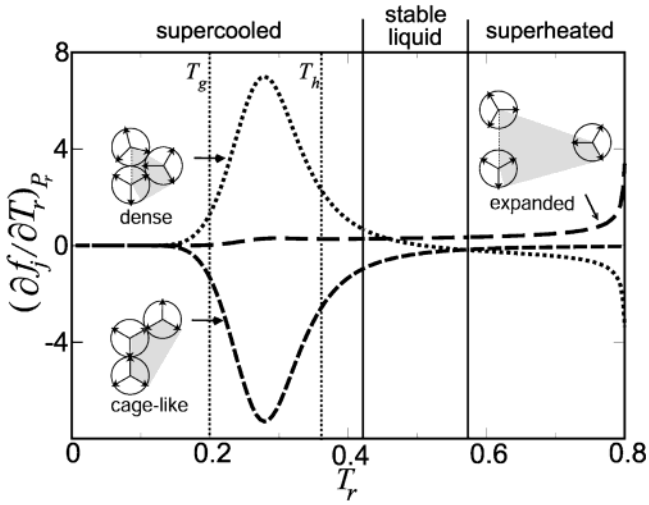

Figure 11. Temperature derivative of the cell populations $(\partial f_j/\partial T_r)_{P_r}$ for the ($j = 1$) cage-like, ($j = 2$) dense, and ($j = 3$) expanded cell types versus reduced temperature T_r at atmospheric pressure.[66] Note that $\sum_j (\partial f_j/\partial T_r)_{P_r} = 0$. Other labels are given in Figure 7.

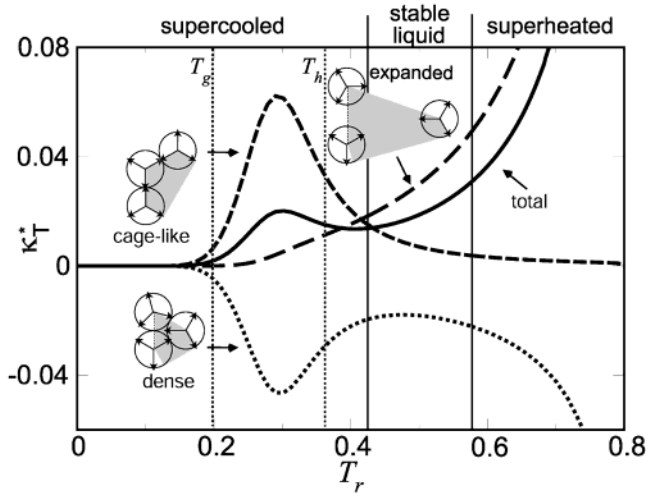

Figure 12. Cell contributions to the liquid's isothermal compressibility $\kappa_{T,j}P_C$ from the ($j = 1$) cage-like, ($j = 2$) dense, and ($j = 3$) expanded cell types versus reduced temperature T_r at atmospheric pressure.[66] The unbroken curve is the total isothermal compressibility $\kappa_T^* = \sum_j \kappa_{T,j}P_C$. Other labels are given in Figure 7.

expansion coefficient in hot and superheated water results from the thermal conversion of dense to expanded structures, increasing the volume with temperature.

Figure 10 illustrates that the pronounced maximum in the heat capacity of the supercooled liquid also arises from the conversion of cages to dense structures, hence the breaking of hydrogen bonds. In the supercooled liquid, raising the temperature melts the hydrogen-bonded cage structures (low enthalpy) into dense structures with van der Waals contacts (higher enthalpy). Because this population change occurs over a relatively small temperature interval, it produces a large heat capacity. The heat capacity subsequently decreases in the stable region because many of the cage-like structures have been melted out. However, near the liquid−vapor spinodal temperature $T_r \approx 0.8025$, both the thermal expansivity and the heat capacity increase dramatically, as the system becomes dominated by fluctuations to the high-volume, high-enthalpy expanded structures.

To understand the individual cell contributions $\alpha_{P,j}$ and $c_{P,j}$, given by eqs 35 and 36, we also show $(\partial f_j/\partial T_r)_{Pr}$ versus T_r in Figure 11. This plot highlights the thermal-induced structural changes mentioned above. Interestingly, in the supercooled liquid, most of the structural transformation occurs in the reduced temperature range $T_g < T_r < T_h$, where the quantities $T_g \approx 0.2$ and $T_h \approx 0.363$ correspond to liquid water's experimental glass transition and homogeneous nucleation temperatures.[6,67]

The isothermal compressibility can also be written as sum of contributions from the cell types $\kappa_T = \sum_j \kappa_{T,j}$ (see eq 34). The $\kappa_{T,j}$ are shown in Figure 12, and the related pressure coefficients of the cell populations $(\partial f_j/\partial P_r)_{T_r}$ are plotted in Figure 13. The behavior of the compressibility can be rationalized using Le Chatelier's principle. In very cold water, the liquid is dominated by rigid cage-like structures, and thus its compressibility is low. As the supercooled liquid is heated, κ_T increases because applied pressure can now collapse the cage-like triplets, disrupting the hydrogen-bond network and forming dense states

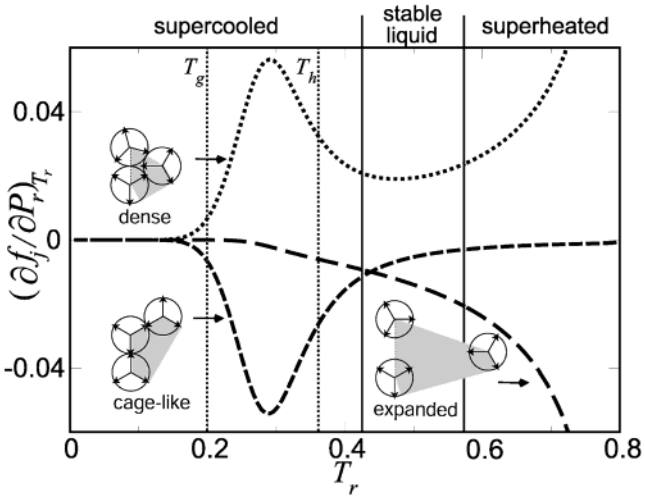

Figure 13. Pressure derivative of the cell populations $(\partial f_j/\partial P_r)_{T_r}$ for the ($j = 1$) cage-like, ($j = 2$) dense, and ($j = 3$) expanded cell types versus reduced temperature T_r at atmospheric pressure.[66] Note that $\sum_j(\partial f_j/\partial P_r)_{T_r} = 0$. Other labels are given in Figure 7.

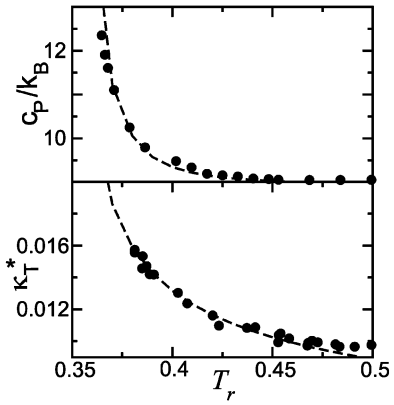

Figure 14. Effect of supercooling on water's thermodynamic response functions at atmospheric pressure: isobaric heat capacity c_P/k_B (top) and isothermal compressibility $\kappa_T^* \equiv -(\partial \ln v_r/\partial P_r)_{T_r}$ (bottom). The circles are experimental data,[84] and the curves are guides to the eye.

with smaller volumes. The stable liquid has a smaller compressibility than the supercooled liquid because many of the open cage-like structures have given way to incompressible dense states. Finally, the isothermal compressibility of hot and superheated water is high because of the presence of low-density (i.e., compressible) expanded structures.

D. Structural Relaxation and the Proposed "Fragile-to-Strong" Transition in Water. If crystallization can be avoided when it is cooled, liquid water (like virtually all liquids) will form a glass.[5] As the temperature is lowered toward the glass transition, its structural relaxation time τ increases rapidly, approaching 10^2 s. Accordingly, its viscosity $\eta \propto \tau$ increases and its diffusivity $D \propto \tau^{-1}$ decreases.

Angell[68,69] has advanced a useful classification for the temperature-dependent relaxation behavior of glass-forming fluids. Liquids that show Arrhenius behavior are called "strong"; those that exhibit marked deviations from Arrhenius behavior are called "fragile". Strong substances, such as the network formers SiO_2 and GeO_2, are able to resist thermal degradation; i.e., their short- and intermediate-range structural order persists to high temperature. On the other hand, key structural features of fragile glass formers, such as *o*-terphenyl, disappear rapidly upon heating above their glass transition temperature.

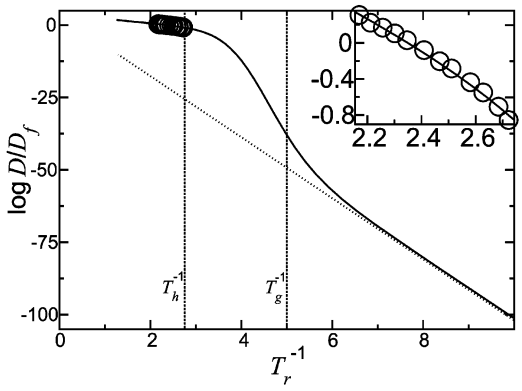

Figure 15. log D/D_f versus reciprocal reduced temperature T_r^{-1}, where D is the self-diffusion coefficient of the liquid and D_f is its value at the freezing transition. The unbroken curve shows the model predictions using the Adam−Gibbs theory (eq 52). The ratio D/D_f depends on one free parameter C, which we set to $C = 12$ to fit the experimental data[78] (circles) at atmospheric pressure.[66] The broken slanted line is provided to highlight the crossover from Arrhenius to non-Arrhenius kinetics in the supercooled liquid, i.e., a fragile-to-strong transition. The vertical dashed lines labeled T_g^{-1} and T_h^{-1} show the location of the experimental[6] glass transition and homogeneous nucleation reciprocal temperatures for liquid water.

Water may be a notable exception to this classification.[70,71] Specifically, supercooled water behaves like a fragile liquid near its freezing temperature, whereas recent evidence indicates that it behaves like a strong liquid near its glass transition temperature.[70,72] It has been proposed that water's unusual relaxation behavior may be directly related to its low-temperature thermodynamic anomalies.[70,73−75] Convincing evidence of this can be found in recent computer simulations by Jagla.[75] The model pair potential used in Jagla's studies is extremely simple, consisting of only a short-range mildly repulsive ramp.[76] This interaction promotes two different local environments, a dense environment (favored at high pressure) and an open environment (favored at low pressure). Despite its simplicity, Jagla's model captures many of water's thermodynamic anomalies and the fragile-to-strong crossover in the temperature-dependence of its diffusivity.

To predict water's kinetics from our thermodynamic model, we use Adam−Gibbs theory,[77] which relates the diffusivity D to the liquid's configurational entropy s_C:

$$D = D_0 \exp\left(-\frac{C}{Ts_c}\right) \tag{52}$$

Here D_0 and C are constants and s_c is usually taken to be the difference between the entropy of the supercooled liquid and the stable crystal at the same temperature and pressure. Starr et al.[73] have used experimental measurements of the entropy, heat capacity, and enthalpy of both liquid and glassy water to construct a thermodynamically plausible form of s_c over a broad range of conditions, including the experimentally inaccessible region below water's homogeneous nucleation temperature. Their analysis suggests that, within the context of the Adam-Gibbs theory, the proposed fragile-to-strong transition is consistent with the available experimental data for water.

Our model gives the entropy of all phases, hence the configurational entropy s_c. Combined with the Adam−Gibbs theory, this allows us to compute the diffusivity D of the supercooled liquid. Figure 15 compares the predictions of our theory at atmospheric pressure[66] to the experimental data.[78] The model predicts a fragile-to-strong transition in supercooled water.

To the extent that water's dynamics are determined by its configurational entropy, as is supposed in the Adam−Gibbs treatment, the present model gives the following explanation for the fragile-to-strong transition. In the coldest supercooled liquid, the dynamics are due to small torsional fluctuations of hydrogen-bonded cage-like structures. The onset of the non-Arrhenius, or fragile, behavior occurs over the reduced temperature range $T_g < T_r < T_h$, where pronounced structural transformations take place in the liquid (see Figure 7). The fragility of the model liquid over this range is due to the large increase in configurational entropy that occurs when the orientationally constrained cage-like structures are melted out, giving way to the orientationally free dense and expanded states. The mobility of water increases sharply with temperature in this range. Once the cages have melted out, further increases in temperature lead only to small increments in mobility, again following near-Arrhenius behavior. This model supports the view[71] that other network-forming substances (including SiO2, BeF_2, and Si) may also have fragile-to-strong transitions.

E. Structural Order Parameters for Liquid Water. Recently, Errington and Debenedetti[39] have studied a translational and an orientational order parameter for characterizing short-range order in liquid water. Their computer simulations[39] of SPC/E water[79] show a "structurally anomalous" region on the phase diagram where, in contrast to simple fluids,[80,81] the translational order and orientational order of the liquid decrease with increasing density. They show that this region contains, as a subset, the conditions where water exhibits anomalous thermodynamic and kinetic behavior.[39,82]

The translational order parameter t of Errington and Debenedetti reflects the tendency of pairs of molecules to adopt preferential separations. The orientational order parameter q reflects the preference of neighboring molecules to be located at specific angles with respect to each other. These order parameters were designed to be small in the disordered gas phase and large in ice I_h.

We explore similar order parameters in our model. We define a translational order parameter t,

$$t = \frac{\langle L_{AC}\rangle^2}{\langle L_{AC}{}^2\rangle} = \frac{[\sqrt{3}f_1 + f_2]^2}{3f_1 + f_2} \tag{53}$$

Here, L_{AC} represents the distance between molecules A and C in cell types 1 and 2. The right-hand side of eq 53 is derived by assuming the minimum energy geometry for each of the two cell types. By this definition, $t = 1$ when all cells are cage-like or dense, and $t = 0$ in the low-density gas (where $f_3 \to 1$, $f_1 \to 0$, $f_2 \to 0$).

We define an orientational order parameter q,

$$q = \left\langle \frac{\cos[3\psi_{ABC}]}{3} + \frac{2\cos[6\psi_{ABC}]}{3} \right\rangle = f_1 + \frac{f_2}{3} \tag{54}$$

where ψ_{ABC} is the angle that describes the triplet ABC of molecular centers in cells of types 1 and 2. Once again, the right-hand side is derived by assuming the minimum energy geometry in each cell. Its limits are $q = 1$ for all molecules in the cage-like structure, $q = 1/3$ for all molecules in the dense structure, and $q = 0$ for all molecules in the expanded structure.

Figure 16 shows t and q versus reduced density for seven isotherms in the supercooled liquid. We find a range of temperature and density where the fluid is "structurally anomalous" by Errington and Debenedetti's criteria: t and q decrease with increasing density. Moreover, these conditions largely coincide with the region on the phase diagram where the fluid exhibits both negative thermal expansion coefficient ($\alpha_p^* < 0$) and the fragile-to-strong transition, confirming the connection between structural, thermodynamic, and kinetic anomalies in water.

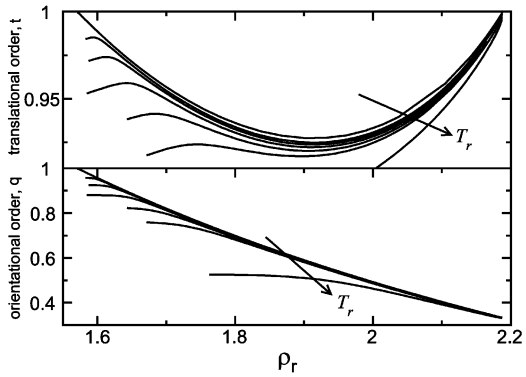

Figure 16. Translational and orientational order parameters t and q, respectively, versus reduced density ρ_r for the supercooled liquid. The curves are for reduced temperatures $T_r = 0.174$, 0.232, 0.247, 0.261, 0.278, 0.299, and 0.348.

However, in contrast to the results of Errington and Debenedetti, we do not find that there is a well-defined "cascade of anomalies" for this model. For example, the TMD does not lie entirely within the structurally anomalous region on the phase diagram. It is not clear whether this is due to the simplifications of our theory or a sign that the cascade of anomalies found in SPC\E is not a generic feature of water models.

IV. Concluding Remarks

We have introduced a model of water in its liquid and solid phases. The model treats van der Waals attractions, steric repulsions, and orientation-dependent hydrogen bonding between neighboring water molecules. It parses water's local structural environments into three classes: cage-like, dense, and expanded structures. This local division captures the connections between energy, volume, and entropy that we believe to be important for water. It is analytical, and thus it offers simple insights into water's behavior, including density maxima, anomalously large heat capacity, minima in both isothermal compressibility, and heat capacity upon isobaric cooling, expansion upon freezing at low pressure, and the conjectured first-order transition between low-temperature amorphous forms. The theory also captures qualitatively the proposed fragile-to-strong transition in the temperature dependence of supercooled water's relaxation processes (e.g., its diffusivity). The success of the model suggests that the unusual properties of water arise from the balance between simple centrosymmetric intermolecular attractions and repulsions, on one hand, and the orientation-dependent hydrogen bonds that impose geometric constraints on the molecular arrangements, on the other.

Acknowledgment. We thank the National Institutes of Health for support.

Appendix A: Connecting the Thermodynamic Response Functions to Fluctuations

The thermodynamic response functions are related to standard fluctuation expressions. For example, at fixed *NPT*, a fluid's thermal expansion coefficient α_P, its isobaric heat capacity c_P, and its isothermal compressibility κ_T are related to the equilibrium fluctuations in enthalpy H and volume V:[83]

$$\alpha_P \equiv \frac{\langle \delta H \delta V \rangle_{NPT}}{V k_B T^2}$$

$$c_P \equiv \frac{\langle \delta H \delta H \rangle_{NPT}}{k_B T^2}$$

$$\kappa_T \equiv \frac{\langle \delta V \delta V \rangle_{NPT}}{V k_B T} \tag{A1}$$

where $\delta H = H - \langle H \rangle_{NPT}$, $\delta V = V - \langle V \rangle_{NPT}$, and the angular brackets indicate averages in the isothermal−isobaric ensemble. Each of these response functions exhibits anomalous temperature dependencies in liquid water. Although eq A1 provides a connection to macroscopic fluctuations, we are interested here in the *microscopic basis* for water's distinctive behavior. We can determine this in our model by evaluating the pressure and temperature derivatives in eqs 26−28 for the thermal expansion coefficient α_P,

$$\begin{aligned}\alpha_P &= \frac{1}{v}\left[\frac{\partial v}{\partial T}\right]_P \\ &= \frac{1}{v}\sum_{j=1}^{3} f_j v_j \left\{\left[\frac{\partial \ln f_j}{\partial T}\right]_P + \left[\frac{\partial \ln v_j}{\partial T}\right]_P\right\} \\ &= \frac{1}{v}\sum_{j=1}^{3} f_j \left\{\frac{h_j v_j - h v}{k_B T^2} + \left[\frac{\partial v_j}{\partial T}\right]_P\right\} \\ &= \frac{1}{v}\frac{\langle \delta h_j \delta v_j \rangle}{k_B T^2} + \frac{1}{v}\left\langle \left[\frac{\partial v_j}{\partial T}\right]_P \right\rangle \end{aligned} \tag{A2}$$

the heat capacity c_P,

$$\begin{aligned} c_P &= \left[\frac{\partial h}{\partial T}\right]_P = \sum_{j=1}^{3} f_j h_j \left\{\left[\frac{\partial \ln f_j}{\partial T}\right]_P + \left[\frac{\partial \ln h_j}{\partial T}\right]_P\right\} \\ &= \sum_{j=1}^{3} f_j \left\{\frac{h_j^2 - h^2}{k_B T^2} + \left[\frac{\partial h}{\partial T}\right]_P\right\} \\ &= \frac{\langle \delta h_j \delta h_j \rangle}{k_B T^2} + \left\langle \left[\frac{\partial h}{\partial T}\right]_P \right\rangle \end{aligned} \tag{A3}$$

and the isothermal compressibility κ_T,

$$\begin{aligned}\kappa_T &= -\frac{1}{v}\left[\frac{\partial v}{\partial P}\right]_T = -\frac{1}{v}\sum_{j=1}^{3} f_j v_j \left\{\left[\frac{\partial \ln f_j}{\partial P}\right]_T + \left[\frac{\partial \ln v_j}{\partial P}\right]_T\right\} \\ &= \frac{1}{v}\sum_{j=1}^{3} f_j \left\{\frac{v_j^2 - v^2}{k_B T} - \left[\frac{\partial v_j}{\partial P}\right]_T\right\} \\ &= \frac{1}{v}\frac{\langle \delta v_j \delta v_j \rangle}{k_B T} - \frac{1}{v}\left\langle \left[\frac{\partial v_j}{\partial P}\right]_T \right\rangle \end{aligned} \tag{A4}$$

In eqs A2−A4, we have $\delta v_j = v_j - v$, $\delta h_j = h_j - h$, and the angular brackets indicate an average over the cell populations $\langle \bullet \rangle = \sum_{j=1}^{3} f_j \bullet$. Each of these expressions contains two terms. The first term, giving microscopic fluctuations, describes changes in the populations of the various cell types. The second term characterizes changes in properties of the individual cells.

Appendix B: Thermodynamic Implications of the Mean-Field Dispersion Term

To understand the thermodynamic implications of "turning on" a mean-field dispersion energy of strength $-Na/v$, consider two systems that have the same number of molecules N and occupy the same volume V at temperature T. One system is the reference system with potential energy $U_0(\mathbf{r}^N)$, and the other system has this potential energy plus the additional mean-field dispersion term,

$$U(\mathbf{r}^N) = U_0(\mathbf{r}^N) - Na/v \tag{B1}$$

We can write the canonical partition function $Q(N,V,T)$ of the latter system as

$$\begin{aligned} Q(N,V,T) &= \frac{c(T)}{N!}\int d\mathbf{r}^N \exp[-U(\mathbf{r}^N)/k_B T] \\ &= \frac{c(T)}{N!}\int d\mathbf{r}^N \exp[-\{U_0(\mathbf{r}^N) - Na/v\}/k_B T] \\ &= \exp\left[\frac{Na}{v k_B T}\right]\frac{c(T)}{N!}\int d\mathbf{r}^N \exp[-U_0(\mathbf{r}^N)/k_B T] \\ &= \exp\left[\frac{Na}{v k_B T}\right] Q_0(N,V,T) \end{aligned} \tag{B2}$$

where $c(T)$ is the momentum contribution to the partition function and $Q_0(N,V,T)$ is the partition function of the reference system. The relationship between their respective Helmholtz free energies A and A_0 is given by the following:

$$A = -k_B T \ln Q = -k_B T \ln Q_0 - Na/v = A_0 - Na/v \tag{B3}$$

Similarly, we can determine the effect of the dispersion potential on the pressure,

$$P = -\left(\frac{\partial A}{\partial V}\right)_{N,T} = -\left(\frac{\partial A_0}{\partial V}\right)_{N,T} - \frac{N^2 a}{V^2} = P_0 - \frac{a}{v^2} \tag{B4}$$

the entropy,

$$S = -\left(\frac{\partial A}{\partial T}\right)_{N,V} = -\left(\frac{\partial A_0}{\partial T}\right)_{N,V} = S_0 \tag{B5}$$

and the chemical potential,

$$\begin{aligned}\mu &= A/N + PV/N = A_0 - a/v + P_0 V/N - a/v \\ &= \mu_0 - 2a/v \end{aligned} \tag{B6}$$

These relationships provide the basis for incorporating the uniform dispersion potential into our model.

References and Notes

(1) For instance, nonmetallic hydrides such as ammonia or methane.

(2) At 1 bar, the minima in liquid water's isobaric heat capacity and isothermal compressibility occur at 36 and 46.5 °C, respectively. The temperature of maximum refractive index is just below 0 °C.

(3) Water's viscosity decreases, and thus its molecular mobility increases, with pressure for temperatures below 33 °C.

(4) Angell, C. A. *Annu. Rev. Phys. Chem.* **1983**, *34*, 593−630.

(5) Debenedetti, P. G. *Metastable Liquids*; Princeton University Press: Princeton, NJ, 1996.

(6) Mishima, O.; Stanley, H. E. *Nature* **1998**, *396*, 329−335.

(7) Kauzmann, W. *Adv. Protein Chem.* **1959**, *14*, 1−63.

(8) Tanford, C. *The Hydrophobic Effect* − Formation of Micelles and Biological Membranes; Wiley-Interscience: New York, 1973.

(9) Dill, K. A. *Biochemistry* **1990**, *29*, 7133−7155.

(10) Hummer, G.; Garde, S.; Garcia, A. E.; Paulaitis, M. E.; Pratt, L. R. *J. Phys. Chem. B* **1998**, *102*, 10469−10482.
(11) Lipowsky, R., Sackmann, E., Eds. *Structure and Dynamics of Membranes*; Vols. 1A and 1B in Handbook of Biological Physics; Elsevier: Amsterdam, 1995.
(12) Kuntz, I. D.; Chen, K.; Sharp, K. A.; Kollman, P. A. *Proc. Natl. Acad. Sci. U.S.A.* **1999**, *96*, 9997−10002.
(13) Pratt, L. R.; Chandler, D. *J. Chem. Phys*. **1977**, *67*, 3683−3704.
(14) Garde, S.; Hummer, G.; Garcia, A. E.; Paulaitis, M. E.; Pratt, L. R. *Phys. Rev. Lett.* **1996**, *77*, 4966−4968.
(15) Lum, K.; Chandler, D.; Weeks, J. D. *J. Phys. Chem. B* **1999**, *103*, 4570−4577.
(16) Ashbaugh, H. S.; Truskett, T. M.; Debenedetti, P. G. *J. Chem. Phys* **2002**, *116*, 2907−2921.
(17) Truskett, T. M.; Dill, K. A. *J. Chem. Phys.* **2002**, *117*, 5101−5104.
(18) Ben-Naim, A. *J. Chem. Phys*. **1971**, *54*, 3682−3695. Ben-Naim, A., *Mol. Phys.* **1972**, *24*, 705−721.
(19) Truskett, T. M.; Debenedetti, P. G.; Sastry, S.; Torquato, S. *J. Chem. Phys.* **1999**, *111*, 2647−2656.
(20) Truskett, T. M.; Debenedetti, P. G.; Torquato, S. *J. Chem. Phys*. **2001**, *114*, 2401−2418.
(21) Silverstein, K. A. T.; Haymet, A. D. J.; Dill, K. A. *J. Am. Chem. Soc.* **1998**, *120*, 3166−3175.
(22) Silverstein, K. A. T.; Dill, K. A.; Haymet, A. D. J. *Fluid Phase Equilib.* **1998**, *151*, 83−90.
(23) Silverstein, K. A. T.; Haymet, A. D. J.; Dill, K. A. *J. Chem. Phys.* **1999**, *111*, 8000−8009.
(24) Silverstein, K. A. T.; Haymet, A. D. J.; Dill, K. A. *J. Am. Chem. Soc.* **2000**, *122*, 8037−8041.
(25) Southall, N. T.; Dill, K. A. *J. Phys. Chem. B* **2000**, *104*, 1326−1331.
(26) Urbic, T.; Vlachy, V.; Kalyuzhnyi, Yu. V.; Southall, N. T.; Dill, K. A. *J. Chem. Phys.* **2000**, *112*, 2843−2848.
(27) Silverstein, K. A.T; Dill, K. A.; Haymet, A. D. J. *J. Chem. Phys.* **2001**, *114*, 6303−6314.
(28) Hill, T. L. *Statistical Mechanics: Principles and Selected Applications*; Dover: New York, 1956.
(29) Hirschfelder, J. O.; Curtiss, C. F.; Bird, R. B. *Molecular Theory of Gases and Liquids*; Wiley: New York, 1954.
(30) Barker, J. A. *Lattice Theories of the Liquid State*; Macmillan: New York, 1963.
(31) Somer, F. L.; Kovac, J. *J. Chem. Phys.* **1994**, *101*, 6216−6221.
(32) Somer, F. L.; Kovac, J. *J. Chem. Phys.* **1995**, *102*, 8995−9004.
(33) Hoover, W. G.; Ashurst, W. T.; Grover, R. *J. Chem. Phys.* **1972**, *57*, 1259−1262.
(34) Gay, S. C.; Rainwater, J. C.; Beale, P. D. *J. Chem Phys.* **2000**, *112*, 9841−9848.
(35) Gay, S. C.; Rainwater, J. C.; Beale, P. D. *J. Chem Phys.* **2000**, *112*, 9849−9859.
(36) Stillinger, F. H. *Science* **1980**, *209*, 451−457
(37) Ball, P. *Life's Matrix: A Biography of Water*; Farrar, Straus, and Giroux: New York, 2000.
(38) Tanaka, H. *Phys. Rev. Lett.* **1999**, *80*, 5750−5753.
(39) Errington, J. R.; Debenedetti, P. G. *Nature* **2001**, *409*, 318−321.
(40) Poole, P. H.; Sciortino, F.; Essman, U.; Stanley, H. E. *Nature* **1992**, *360*, 324−328.
(41) Poole, P. H.; Essmann, U.; Scortino, F; Stanley, H. E. *Phys. Rev. E* **1993**, *48*, 4605−4610.
(42) Harrington, S.; Zhang, R.; Poole, P. H.; Sciortino, F.; Stanley, H. E. *Phys. Rev. Lett.* **1997**, *78*, 2409−2412.
(43) Shiratani, E.; Sasai, M. *J. Chem. Phys.* **1998**, *108*, 3264−3276.
(44) Paschek, D.; Geiger, A. *J. Phys. Chem. B* **1999**, *103*, 4139−4146.
(45) Bellissent-Funel, M. C. *Europhys. Lett.* **1998**, *42*, 161−166.
(46) Canpolat, M.; et al. *Chem. Phys. Lett.* **1998**, *294*, 9−12.
(47) The terms "structured" and "unstructured" are purely descriptive and are introduced to characterize the bimodal character of the local packing arrangements in liquid water.[6,39]
(48) Note that the large ratio of k_s to ϵ_{HB} used in Table 2 provides some justification for this approximation. An alternative approach that would permit an analytical solution of our model would be to expand the cell volume in a Taylor series, $v_1(\theta) \approx 3\sqrt{3}d^2/4 - 3\sqrt{3}(\theta - 2\pi/3)^2\, d^2/16 +$ ..., and retain the first two terms.
(49) For classical two-dimensional systems, $c(T) = (2\pi m k_B T/h^2) q(T)$, m is the molecular mass, h is Planck's constant, and $q(T)$ is the internal partition function for a single particle that may contain contributions from rotational, vibrational, electronic, and nuclear degrees of freedom. For our simple two-dimensional model, we incorporate only the rotational contribution to the internal partition function, which scales as $q(T) \propto T^{1/2}$.
(50) Jagla, E. A. *J. Chem. Phys.* **1999**, *111*, 8980−8986.
(51) Paras, E. P. A.; Vega, C.; Monson, P. A. *Mol. Phys.* **1993**, *70*, 1063−1072.
(52) Vega, C.; Monson, P. A. *Mol. Phys.* **1995**, *85*, 413−421.
(53) Gay, S. C.; Beale, P. D.; Rainwater, J. C. *J. Chem. Phys.* **1998**, *109*, 6820−6827.
(54) Malanoski, A. P.; Vega, C.; Monson, P. A. *Mol. Phys.* **2000**, *98*, 363−370.
(55) Löwen, H. *Phys. Rep.* **1994**, *237*, 249−324.
(56) Petrenko, V. F.; Whitworth, R. W. *Physics of Ice*; Oxford University Press: New York, 1999.
(57) Báez, L. A.; Clancy, P. *J. Chem. Phys.* **1995**, *103*, 9744−9755. Rick, S. W. *J. Chem. Phys.* **2001**, *114*, 2276−2283. Arbuckle, B. W.; Clancy, P. *J. Chem. Phys.* **2002**, *116*, 5090−5098.
(58) Voronoi, G. F. *J. Reine Agnew. Math.* **1908**, *134*, 198−287.
(59) In practice, the pressure−temperature coordinates of the phase boundaries were found by setting the expressions for μ of two phases equal, choosing a temperature, and using a simple iterative scheme to find the value of pressure that satisfies the equality. The expressions for the chemical potentials of the fluid, LP, and HP phases are given by eqs 31, 46, 51, respectively.
(60) Strandburg, K. J. *Rev. Mod. Phys.* **1988**, *60*, 161−207.
(61) Glaser, M. A.; Clark, N. A. *Adv. Chem. Phys.* **1993**, *83*, 543−709.
(62) Mishima, O.; Calvert, L. D.; Whalley, E. *Nature* **1985**, *314*, 76−78.
(63) Mishima, O. *J. Chem. Phys.* **1994**, *100*, 5910−5912.
(64) Because glasses are not in thermodynamic equilibrium, the experimental transformation between LDA and HDA is not a true phase transition. However, the sharp changes in volume and enthalpy that accompany the transformation give it a "first-order" character.
(65) Debenedetti, P. G. *Nature* **1998**, *392*, 127.
(66) We choose the model's "atmospheric" pressure to be $P_r^{atm} = 0.1627$, where it exhibits a reduced freezing temperature of $T_r \approx 0.4255$ and a reduced boiling temperature of $T_r \approx 0.5804$. Inputting water's critical parameters yields a freezing temperature of 2.2 °C and a boiling temperature of 102.4 °C. Thus, at "atmospheric" pressure P_r^{atm}, the model liquid displays approximately the same range of thermodynamic stability as does liquid water at 1 atm.
(67) The range of temperatures $T_g < T_r < T_h$ has been referred to as the "no man's land" for liquid water because, under those conditions, rapid crystallization prevents experimental access to the supercooled liquid.
(68) Angell, C. A. *J. Non-Cryst. Solids* **1991**, *131*−*133*, 13−31.
(69) Angell, C. A. *Science* **1995**, *267*, 1924−1935.
(70) Ito, K.; Moynihan, C. T.; Angell, C. A. *Nature* **1999**, *398*, 492−495.
(71) Angell, C. A.; Bressel, R. D.; Hemmati, M.; Sare, E. J.; Tucker, J. C. *Phys. Chem. Chem. Phys.* **2000**, *2*, 1559−1566.
(72) This is still a matter of scientific debate. In particular, the recent diffusivity measurements of Smith and Kay (Smith, R. S.; Kay, B. D. *Nature* **1999**, *398*, 788−791) appear to contradict the notion that water is "strong" near its glass transition.
(73) Starr, F. W.; Angell, C. A.; Speedy, R. J.; Stanley, H. E. LANL preprint #9903451.
(74) Jagla, E. A. *J. Phys.: Condens. Matt.* **1999**, *11*, 10251−10258.
(75) Jagla, E. A. *Mol. Phys.* **2001**, *99*, 753−757.
(76) Size polydispersity was also added to the pair potential in order prevent crystallization at low temperature.
(77) Adam. G.; Gibbs, J. H. *J. Chem. Phys.* **1965**, *43*, 139−146.
(78) Price, W. S.; Ide, H.; Arata, Y. *J. Phys. Chem. A* **1999**, *103*, 448−450.
(79) Berendsen, H. J. C.; Grigera, R. J.; Stroatsma, T. P. *J. Phys. Chem.* **1987**, *91*, 6269−6271.
(80) Torquato, S.; Truskett, T. M.; Debenedetti, P. G. *Phys. Rev. Lett.* **2000**, *84*, 2064−2067.
(81) Truskett, T. M.; Torquato, S.; Debenedetti, P. G. *Phys. Rev. E* **2000**, *62*, 993−1001.
(82) Sastry, S. *Nature* **2001**, *409*, 300−301.
(83) See, e.g.: Landau, L. D.; Lifshitz, E. M. *Statistical Physics*, 3rd ed.; Pergamon: Oxford, 1980; Part I, Vol. 5.
(84) Kell, G. S. *J. Chem. Eng. Data* **1967**, *12*, 66−69. Speedy, R. J.; Angell, C. A. *J. Chem. Phys.* **1976**, *65*, 851−858. Angell, C. A.; Oguni, M.; Sichina, W. J. *J. Phys. Chem.* **1982**, *86*, 998−1002. Hare, D. E.; Sorensen, C. M. *J. Chem. Phys.* **1986**, *84*, 5085−5089.